

# We are IntechOpen, the world's leading publisher of Open Access books Built by scientists, for scientists

6,900

Open access books available

186,000

International authors and editors

200M

Downloads

Our authors are among the

154

Countries delivered to

TOP 1%

most cited scientists

12.2%

Contributors from top 500 universities



WEB OF SCIENCE™

Selection of our books indexed in the Book Citation Index  
in Web of Science™ Core Collection (BKCI)

Interested in publishing with us?  
Contact [book.department@intechopen.com](mailto:book.department@intechopen.com)

Numbers displayed above are based on latest data collected.  
For more information visit [www.intechopen.com](http://www.intechopen.com)



# Array Pattern Based on Integrated Antenna

*Daehee Park and Dong-Ho Cho*

## Abstract

The number of required antenna elements is rapidly increasing, in compliance with the development of massive multiple-input multiple-output (MIMO) and beamforming techniques in 5G technology. Integrated antenna, which is composed of multiple antenna elements, will be considered for next-generation technologies. Therefore, in this chapter, we provide the mathematical and practical explanation of the integrated antenna for the next-generation technologies. First, we introduce a mathematical expression of an antenna element based on spherical vector wave modes and explain channel models for the integrated antenna and the antenna array based on the integrated antenna. Second, we provide practical antennas designed as the integrated antenna and verify that the integrated antenna array can be implemented practically. Lastly, we evaluate the performance of the integrated antenna array compared to mono-polarization and dual-polarization dipole arrays.

**Keywords:** integrated antenna, integrated antenna array, spherical vector wave, channel model, practical antenna

## 1. Introduction

As more high speed is required, many 5G communication systems have been proposed. While there are a lot of technologies for the 5G communication system, multiple-input multiple-output (MIMO) system is a basis for the 5G communication system. MIMO system has been proposed to increase spectral efficiency and diversity gain in wireless communication. The MIMO technology enhances the spectral efficiency and diversity gain by utilizing multiple antennas, because the multiple antennas provide multiple channels [1, 2]. In order to obtain multiple channels, the antenna elements have to be separated from the other antenna elements with larger gap than half-wavelength distance. However, it is difficult to increase the number of antennas because the antenna size is limited in wireless communication.

To enhance the spectral efficiency with compact antenna size, dual-polarization antenna array has been used for 5G technology [3]. It is possible to obtain two uncorrelated channels using the orthogonality of the dual-polarization antenna. However, the dual-polarization antenna still has limitation to increase the spectral efficiency without expanding antenna space.

It has been studied to enhance the spectral efficiency without increasing antenna space by using multiple radiation patterns of the antennas [4–7]. It was theoretically proposed that six times of spectral efficiency can be obtained compared to a single antenna by using three electric dipoles and three magnetic dipoles allocated at the same position. It means that the multiple antennas can be integrated within a compact size and provide multiplexing gain. Thus, the MIMO system can increase the spectral efficiency by not only using larger antenna array size but also combining multiple radiation patterns.

On the other hand, there have been studies of array optimization technologies for the linear antenna array according to various objective functions [8, 9]. This antenna array could have better interference cancelation using genetic algorithms. Then, it is also possible to enhance the spectral efficiency and diversity gain by combining the array optimization technologies and the integrated antenna-based array system.

In this chapter, we introduce an integrated antenna array which is a type of the MIMO systems. The integrated antenna array consists of multiple array elements, and the array element has multiple antenna elements. Each antenna element of the integrated antenna has different radiation patterns to increase the spectral efficiency in wireless communication area. The purpose of this chapter is to introduce the concept of the integrated antenna array and to show the possibility to apply it practically to wireless communication technology. We will also explain a framework for next-generation technology so that we can provide further works as well.

We organize the chapter as follows. In Section 2, we explain channel models for the integrated antenna array. In Section 3, several practical integrated antennas are introduced to verify that the integrated antenna array can be implemented practically. In Section 4, we verify the performance of the integrated antenna array in urban macro-cell environment compared with mono-polarization and dual-polarization dipole antenna arrays.

## 2. Channel model

The channel model is dependent on the structure of the MIMO system. To provide the channel model for the integrated antenna array, firstly we provide a channel model for a general case as given in **Figure 1** [1]. We develop the channel model with considering complex structures.

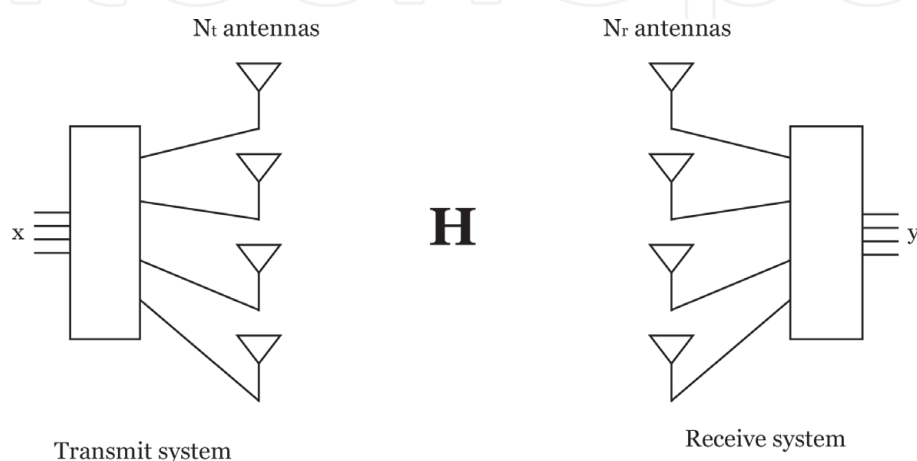


**Figure 1.**  
Configuration of general MIMO system.

## 2.1 MIMO channel model

We consider a MIMO channel with a transmit and receive system, which is equipped with  $N_t$  antennas and  $N_r$  antennas, respectively. The received signal  $\mathbf{y}$  can be expressed as

$$\mathbf{y} = \mathbf{H}\mathbf{x} + \mathbf{n}, \quad (1)$$

where  $\mathbf{H}$  is the  $N_r \times N_t$  MIMO channel,  $\mathbf{x}$  is an  $N_t \times 1$  transmit signal and  $\mathbf{n}$  is an  $N_r \times 1$  complex Gaussian noise. Based on spatial fading correlation, the elements of  $\mathbf{H}$  can be described as

$$\mathbf{h} = \text{vec}(\mathbf{H}) = \mathbf{R}_h^{1/2} \text{vec}(\mathbf{H}_w), \quad (2)$$

where  $\mathbf{H}_w$  is an  $N_r \times N_t$  Rayleigh fading channel with uncorrelated and zero mean entries which follow complex Gaussian distribution,  $\mathbf{R}_h = \mathbb{E}\{\mathbf{h}\mathbf{h}^\dagger\}$  is the  $N_r N_t \times N_r N_t$  covariance matrix and  $(\cdot)^\dagger$  and  $\mathbb{E}\{\cdot\}$  are Hermitian and expectation operator, respectively [1]. Here,  $\text{vec}(\mathbf{A})$  is a vectorization operation to produce a vector with the columns of  $\mathbf{A}$ .

We assume that the sizes of the transmit and receive antenna are negligible compared to the distance between the transmit system and the receive system. Then, the covariance matrix of the MIMO channel is given by

$$\mathbf{R}_h = \mathbf{R}'_{H_t} \otimes \mathbf{R}_{H_r}, \quad (3)$$

where  $\mathbf{R}_{H_r} = \mathbb{E}\{\mathbf{H}\mathbf{H}^\dagger\}$ ,  $\mathbf{R}'_{H_t} = \mathbb{E}\{\mathbf{H}^\dagger\mathbf{H}\}$  and  $(\cdot)'$  and  $\otimes$  are matrix transpose and Kronecker product operator, respectively. Therefore, the MIMO channel can be described as [1]

$$\mathbf{H} = \mathbf{R}'_{H_r}{}^{1/2} \mathbf{H}_w \mathbf{R}_{H_t}{}^{1/2}. \quad (4)$$

This channel model is called by the Kronecker model of MIMO system in general case.

## 2.2 Spherical vector wave-based channel model

There are spherical vector wave (SVW) modes which are orthonormal basis functions for arbitrary radiation pattern [10–12]. The radiation pattern of an arbitrary transmitter antenna is described as

$$\begin{aligned} \mathbf{F}(\hat{\mathbf{r}}) &= k\sqrt{2\eta} \sum_{l=1}^{l_{\max}} \sum_{\nu=0}^l \sum_{s=1}^2 \sum_{\tau=1}^2 j^{\tau-l+2} T_{l\nu s\tau} \mathbf{A}_{l\nu s\tau}(\hat{\mathbf{r}}) \\ &= k\sqrt{2\eta} \sum_{\alpha=1}^{\alpha_{\max}} j^{\tau-l+2} T_\alpha \mathbf{A}_\alpha(\hat{\mathbf{r}}) = k\sqrt{2\eta} \mathbf{A}'(\hat{\mathbf{r}}) \mathbf{t}, \end{aligned} \quad (5)$$

where  $\hat{\mathbf{r}}$  is the direction of the radiation,  $\mathbf{A}_{l\nu s\tau}(\hat{\mathbf{r}}) = \mathbf{A}_\alpha(\hat{\mathbf{r}}) = [A_{\theta,\alpha}(\hat{\mathbf{r}}) A_{\phi,\alpha}(\hat{\mathbf{r}})]$  is  $\alpha$ th SVW mode with the multi-index  $\alpha = 2(l(l+1) - 1 + (-1)^s \nu) + \tau$ ,  $\alpha_{\max}$  is the maximum number of SVW modes,  $\mathbf{A}(\hat{\mathbf{r}})$  is an  $\alpha_{\max} \times 2$  matrix containing the row vector  $j^{\tau-l+2} \mathbf{A}_\alpha(\hat{\mathbf{r}})$  and  $\mathbf{t}$  is an  $\alpha_{\max} \times 1$  vector with the element  $T_\alpha$  which is the transmitting coefficient of the transmitter antenna [10]. The SVW mode  $\mathbf{A}_\alpha(\hat{\mathbf{r}})$  is described well in Appendix. In order to decompose the radiation pattern of a receiver antenna, the

receiving coefficient  $R_{uv\tau}$  can be given by  $R_{u1\tau} = (-1)^\nu T_{u2\tau}$  and  $R_{u2\tau} = (-1)^\nu T_{u1\tau}$  by using the reciprocity relationship [10, 12].

Consider that the transmit and the receive systems have an integrated antenna without array structure, which are composed of  $N_t$  and  $N_r$  antennas as shown in **Figure 2**, respectively. From (1), the MIMO channel  $\mathbf{H}$  may be expressed as

$$\mathbf{y} = \mathbf{RMT}\mathbf{x} + \mathbf{n}, \quad (6)$$

where  $\mathbf{R}$  is an  $N_r \times M_r$  matrix with the receiving coefficient  $R_{n_r, m_r}$ ,  $\mathbf{T}$  is a  $M_t \times N_t$  matrix with the transmitting coefficient  $T_{m_t, n_t}$  and  $\mathbf{M}$  is a  $M_r \times M_t$  matrix which is the channel between SVW modes [10, 12, 13]. Then, the covariance matrix of the channel  $\mathbf{H}$  can be derived by [14]

$$\mathbf{R}_h = (\mathbf{T}' \otimes \mathbf{R}) \mathbf{R}_m (\mathbf{T}' \otimes \mathbf{R})^\dagger, \quad (7)$$

where  $\mathbf{h} = \text{vec}(\mathbf{H}) = (\mathbf{T}' \otimes \mathbf{R}) \mathbf{m}$ ,  $\mathbf{m} = \text{vec}(\mathbf{M})$  and  $\mathbf{R}_m = \mathbb{E}\{\mathbf{m}\mathbf{m}^\dagger\}$ . The covariance matrix of the channel for the SVW modes can be described as

$$\mathbf{R}_m = 4\pi^2 \iint \tilde{\mathbf{A}}(\hat{\mathbf{k}}_r, \hat{\mathbf{k}}_t) \mathbf{P}(\hat{\mathbf{k}}_r, \hat{\mathbf{k}}_t) \tilde{\mathbf{A}}^\dagger(\hat{\mathbf{k}}_r, \hat{\mathbf{k}}_t) d\Omega_r d\Omega_t. \quad (8)$$

Here,  $\tilde{\mathbf{A}}(\hat{\mathbf{k}}_r, \hat{\mathbf{k}}_t) = \mathbf{A}(\hat{\mathbf{k}}_r) \otimes \mathbf{A}(\hat{\mathbf{k}}_t)$ , and  $\mathbf{P}(\hat{\mathbf{k}}_r, \hat{\mathbf{k}}_t) = \text{diag}(\mathcal{P}_{\theta\theta}, \mathcal{P}_{\theta\phi}, \mathcal{P}_{\phi\theta}, \mathcal{P}_{\phi\phi})$  where  $\mathcal{P}_{\alpha\beta} \equiv \mathcal{P}_{\alpha\beta}(\hat{\mathbf{k}}_r, \hat{\mathbf{k}}_t)$  are functions of the power angular spread (PAS) which is expressed by

$$\mathcal{P}_{\alpha\beta}(\hat{\mathbf{k}}_r, \hat{\mathbf{k}}_t) = P_{\alpha\beta} p_{\alpha\beta}(\hat{\mathbf{k}}_r, \hat{\mathbf{k}}_t), \quad (9)$$

where  $\alpha \in \{\theta, \phi\}$ ,  $\beta \in \{\theta, \phi\}$  and  $P_{\alpha\beta}$  is coupling power from  $\beta$  to  $\alpha$  [15]. The joint probability function  $p_{\alpha\beta}(\hat{\mathbf{k}}_r, \hat{\mathbf{k}}_t)$  is required to be normalized as follows:

$$\iint p_{\alpha\beta}(\hat{\mathbf{k}}_r, \hat{\mathbf{k}}_t) d\Omega_r d\Omega_t = 1. \quad (10)$$

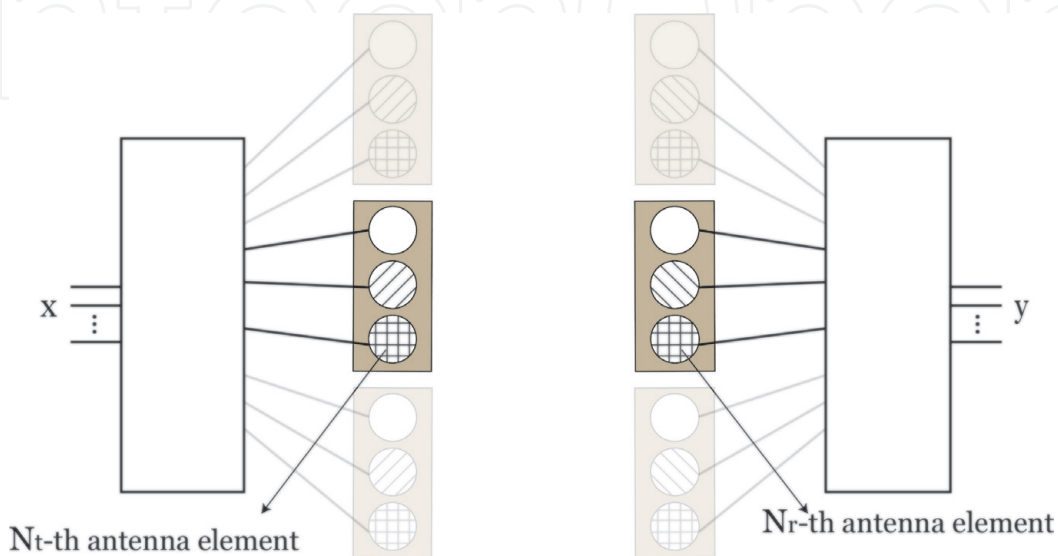


**Figure 2.**  
Configuration of MIMO system with integrated antenna.

It is also assumed that the joint probability density function of the PAS in (10) can be decomposed by

$$p_{\alpha\beta}(\hat{\mathbf{k}}_r, \hat{\mathbf{k}}_t) = p_{\alpha\beta}(\hat{\mathbf{k}}_r) p_{\alpha\beta}(\hat{\mathbf{k}}_t). \quad (11)$$

Then, the SVW mode channel of the transmitter is obtained by [14].

$$\mathbf{R}_{M_t} = 2\pi \int \mathbf{A}^*(\hat{\mathbf{k}}_t) \mathbf{P}(\hat{\mathbf{k}}_t) \mathbf{A}'(\hat{\mathbf{k}}_t) d\Omega_t, \text{ and } \mathbf{R}_{M_r} = 2\pi \int \mathbf{A}^*(\hat{\mathbf{k}}_r) \mathbf{P}(\hat{\mathbf{k}}_r) \mathbf{A}'(\hat{\mathbf{k}}_r) d\Omega_r. \quad (12)$$

where  $\mathbf{P}(\hat{\mathbf{k}}_t) = \text{diag}\{\mathcal{P}_\theta(\hat{\mathbf{k}}_t), \mathcal{P}_\phi(\hat{\mathbf{k}}_t)\}$ ,  $\mathcal{P}_\alpha(\hat{\mathbf{k}}_t) = P_\alpha p_\alpha(\hat{\mathbf{k}}_t)$  and  $p_\alpha(\hat{\mathbf{k}}_t)$  is the PAS of orthogonal polarization  $\alpha$  at transmitter side and  $\alpha$  stands for  $\theta$  and  $\phi$ .

From (3) and (7), therefore, we can see that

$$\mathbf{R}_{H_t} = \mathbf{T}^\dagger \mathbf{R}_{M_t} \mathbf{T}, \mathbf{R}_{H_r} = \mathbf{R} \mathbf{R}_{M_r} \mathbf{R}^\dagger. \quad (13)$$

We can describe the channel model for the integrated antenna by using the SVW modes.

### 2.3 Channel model for integrated antenna array

For 5G communication technology, it is important that the integrated antenna is expandable to array structure. Thus, it is necessary to derive the channel model for the MIMO system equipped with the integrated antenna array. The structure of the integrated antenna array is illustrated in **Figure 3**.

Each antenna element has not only a radiation pattern but also a relative position to the other antenna elements. The received signal of the MIMO system with the integrated antenna arrays is given by

$$\mathbf{y} = \check{\mathbf{R}} \check{\mathbf{M}} \check{\mathbf{T}} \mathbf{x} + \mathbf{n}, \quad (14)$$

where  $\check{\mathbf{M}}$  is the  $M_r L_r \times M_t L_t$  extended SVW mode channel, which considers antenna positions;  $\check{\mathbf{R}} = \mathbf{I}_{L_r} \otimes \mathbf{R}$ , where  $\mathbf{R}$  is an  $B_r \times M_r$  receiving coefficient matrix of the receive integrated antenna; and  $\check{\mathbf{T}} = \mathbf{I}_{L_t} \otimes \mathbf{T}$ , where  $\mathbf{T}$  and  $\mathbf{I}_N$  are a  $M_t \times B_t$

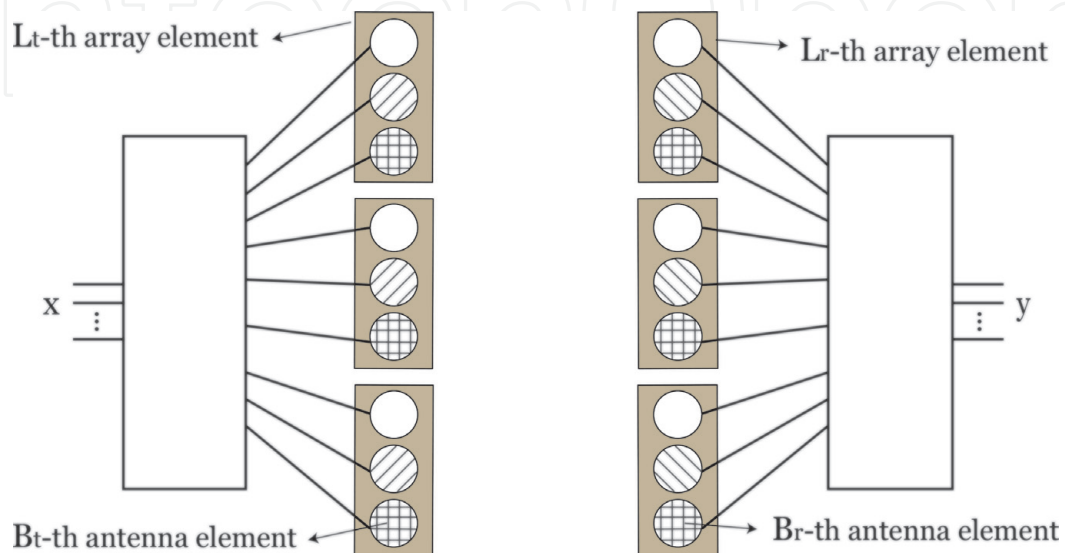


**Figure 3.**  
 Configuration of MIMO system with integrated antenna array.

transmitting coefficient matrix of the transmit integrated antenna and an  $N \times N$  identity matrix. The covariance matrix of the MIMO channel  $\mathbf{H}$  can be described as

$$\mathbf{R}_h = \left( \check{\mathbf{T}}' \otimes \check{\mathbf{R}} \right) \mathbf{R} \check{\mathbf{m}} \left( \check{\mathbf{T}}' \otimes \check{\mathbf{R}} \right)^\dagger, \quad (15)$$

where  $\mathbf{h} = \left( \check{\mathbf{T}}' \otimes \check{\mathbf{R}} \right) \check{\mathbf{m}}$ ,  $\check{\mathbf{m}} = \text{vec}(\check{\mathbf{M}})$  and  $\mathbf{R} \check{\mathbf{m}} = \mathbb{E} \left\{ \frac{\check{\mathbf{m}} \check{\mathbf{m}}^\dagger}{\check{\mathbf{m}}^\dagger \check{\mathbf{m}}} \right\}$ . Here, the correlation matrix of the channel of the SVW modes can be given by

$$\mathbf{R} \check{\mathbf{m}} = 4\pi^2 \iint \tilde{\mathbf{B}}(\hat{\mathbf{k}}_r, \hat{\mathbf{k}}_t) \mathbf{P}(\hat{\mathbf{k}}_r, \hat{\mathbf{k}}_t) \tilde{\mathbf{B}}^\dagger(\hat{\mathbf{k}}_r, \hat{\mathbf{k}}_t) d\Omega_r d\Omega_t, \quad (16)$$

where  $\tilde{\mathbf{B}}(\hat{\mathbf{k}}_r, \hat{\mathbf{k}}_t) = \mathbf{B}(\hat{\mathbf{k}}_r) \otimes \mathbf{B}(\hat{\mathbf{k}}_t)$ . Here,  $\mathbf{B}(\hat{\mathbf{k}}_r) = \mathbf{e}_r(\hat{\mathbf{k}}_r) \otimes \mathbf{A}(\hat{\mathbf{k}}_r)$ , and the  $\mathbf{E}(\hat{\mathbf{k}})$  is an array element response matrix with the elements of  $e_l(\hat{\mathbf{k}}) = e^{j\beta(\mathbf{r}_l - \mathbf{r}_o) \cdot \hat{\mathbf{k}}}$ , where  $\mathbf{r}_l$  is the position of the  $l$ th array element and  $\mathbf{r}_o$  is the position of the antenna array system.

We explained the channel models for the MIMO system with the integrated antenna arrays mathematically. In the following section, we will verify the performance of the integrated antenna array based on the channel model we discussed.

### 3. Practical antenna design

There have been many practical antennas which are designed for the integrated antenna. Through some practical antennas, we can see that the integrated antenna may be implemented for the wireless communication. Design of the integrated antenna is dependent on the system requirement such as array structure and channel environment. In this section, we introduce various practical integrated antennas for several cases.

#### 3.1 Practical integrated antenna

It is important to integrate multiple antennas with compact size, which have orthogonal radiation patterns of each other. There are practical integrated antennas without considering array structure as shown in **Figure 4**. It is found that the integrated antenna has two types of antenna elements which have radiation patterns of electric dipole antenna and magnetic loop antenna. Planer inverted-F antennas (PIFA) are used for the electric dipole antenna, and quarter-wavelength slot antennas are used for the magnetic loop antenna [16, 17]. It is also seen that the integrated antennas have three-dimensional structures because the array structure was not considered. Therefore, it is noted that the integrated antenna may consist of more than two antenna elements practically.

#### 3.2 Practical integrated antenna array

The integrated antenna array may be implemented as shown in **Figure 5**. It is found that the practical integrated antenna array is composed of  $L_t$  array elements. Each array element consists of  $B_t$  antenna elements, which are designed by utilizing a planer Yagi-Uda antenna [18].

To reduce the antenna size, we eliminated a conduct strip in front of the antenna element and designed that  $l_3$  is larger than  $w_2$  as shown in **Figure 5a**. The radiation

direction of the antenna element can be changed according to  $\theta_{\text{rad}}$ , because the antenna element radiates perpendicularly to the antenna structure. The parameters are given by  $L = 70 \text{ mm}$ ,  $W = 66 \text{ mm}$ ,  $l_c = 22 \text{ mm}$ ,  $w_c = 1.5 \text{ mm}$ ,  $l_s = 24.5 \text{ mm}$ ,  $w_s = 1.5 \text{ mm}$ ,  $l_f = 6.2 \text{ mm}$ ,  $w_p = 8 \text{ mm}$  and  $l_p = 32 \text{ mm}$ . It is possible to control the impedance matching by modifying  $l_7$  and  $w_6$ . The integrated antenna is produced on a CER-10 substrate with a permittivity of 10 and a thickness of 0.64 mm. The

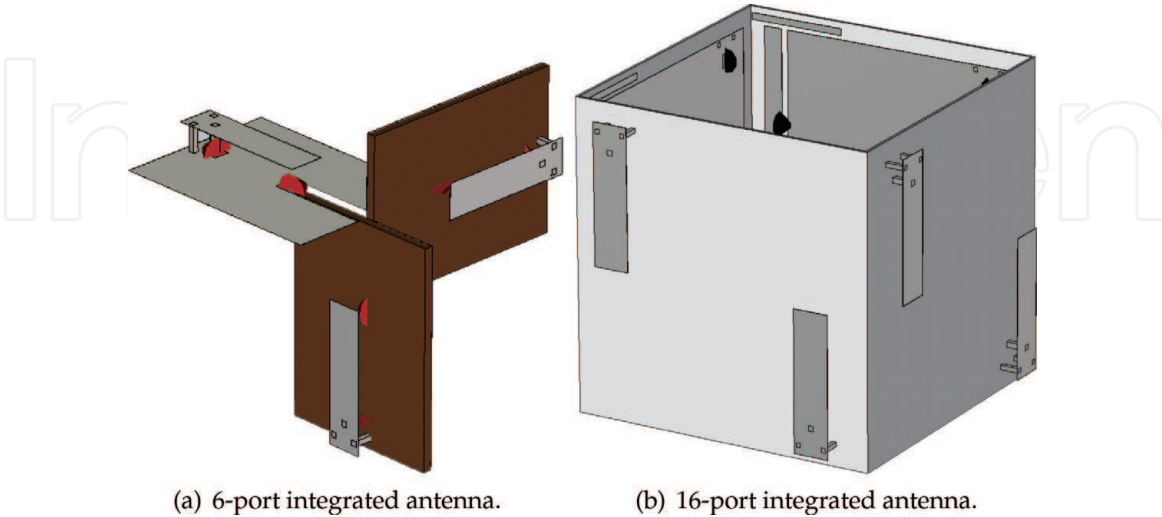


**Figure 4.** Configuration of practical integrated antennas. (a) 6-port integrated antenna and (b) 16-port integrated antenna.

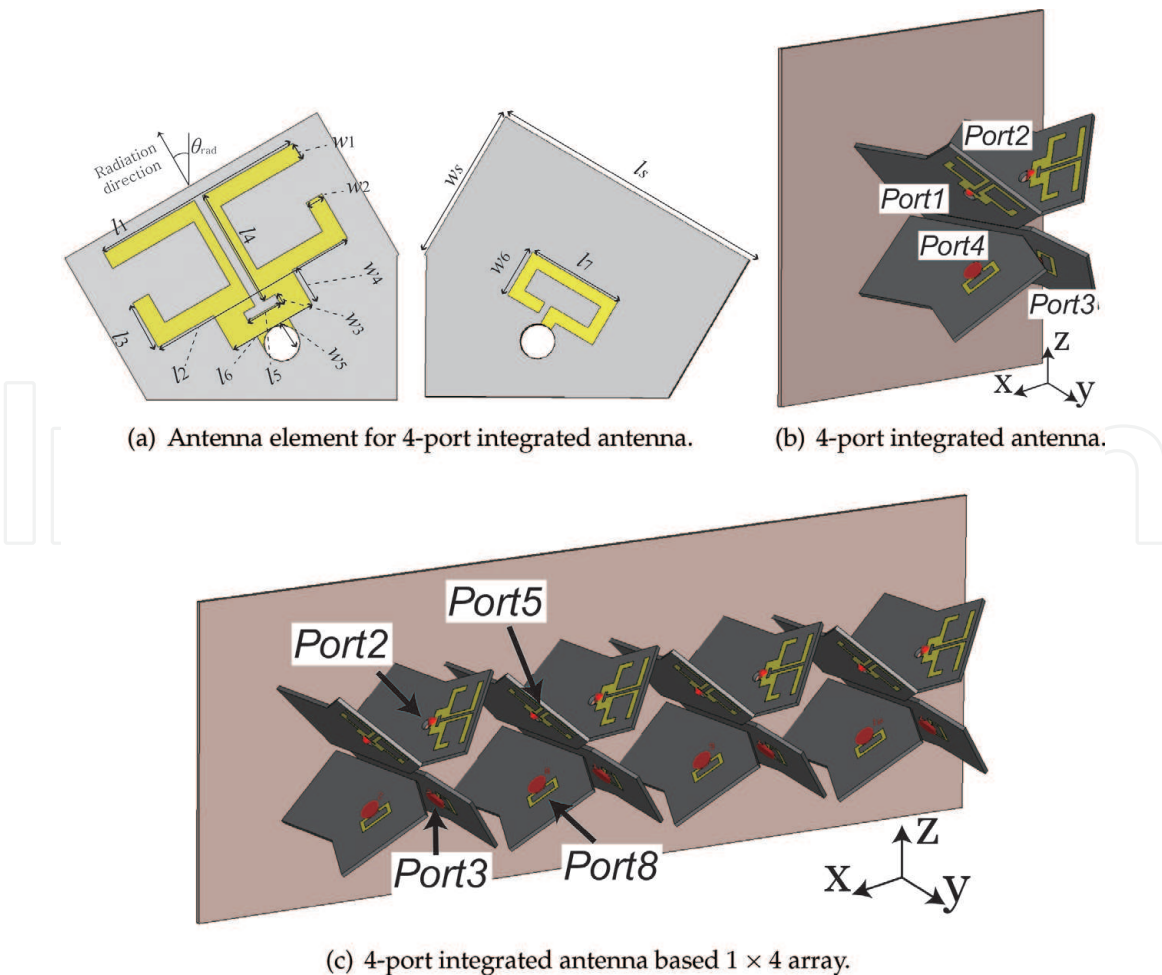


**Figure 5.** Configuration of practical integrated antenna array. (a) Antenna element for 4-port integrated antenna, (b) 4-port integrated antenna and (c) 4-port integrated antenna based  $1 \times 4$  array.

integrated antenna is expandable to the array structure as shown in **Figure 4c**, because of the compactness of the integrated antenna.

It is necessary to verify that the integrated antenna has reasonable antenna characteristics such as radiation efficiency, bandwidth and mutual coupling. The proposed four-port integrated antenna was implemented as shown in **Figure 6**. For the integrated antenna, the antenna elements have the same antenna characteristics of each other because of symmetric configuration. The simulated and the measured S-parameters of the integrated antenna are shown in **Figure 7a** and **b**, respectively, where  $S_{aa}$  means  $S_{1,1}$ ,  $S_{2,2}$ ,  $S_{3,3}$  and  $S_{4,4}$ ;  $S_{ab}$  means  $S_{1,2}$ ,  $S_{1,4}$ ,  $S_{2,3}$  and  $S_{3,4}$ ; and  $S_{ac}$  means  $S_{1,3}$  and  $S_{2,4}$ . The integrated antennas radiate at 5.7 GHz with a bandwidth of about 300 MHz satisfying  $|S_{aa}| = -10$  dB in the simulation and measurement. It is also found that the antenna elements have less than  $-12$  dB mutual couplings in the simulation and measurement.

The simulated and measured S-parameters of the integrated antenna-based  $1 \times 4$  array system are shown in **Figure 8a** and **b**, respectively. Only the S-parameters for *Port 5* are illustrated because the integrated antenna-based array has

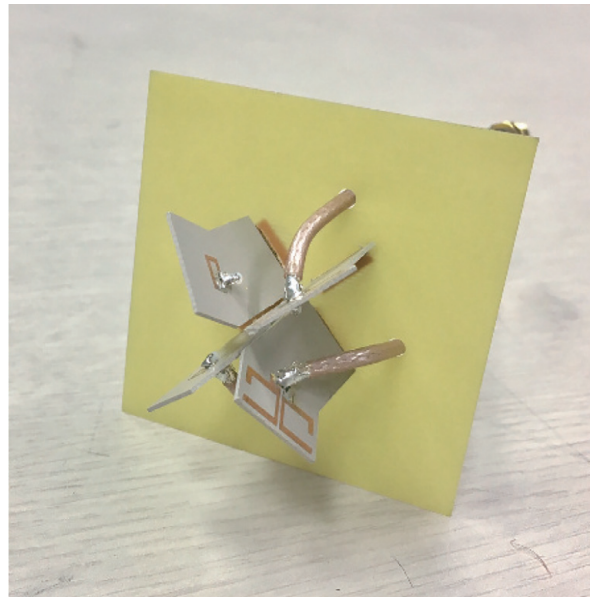


**Figure 6.**  
Prototype of four-port integrated antenna.

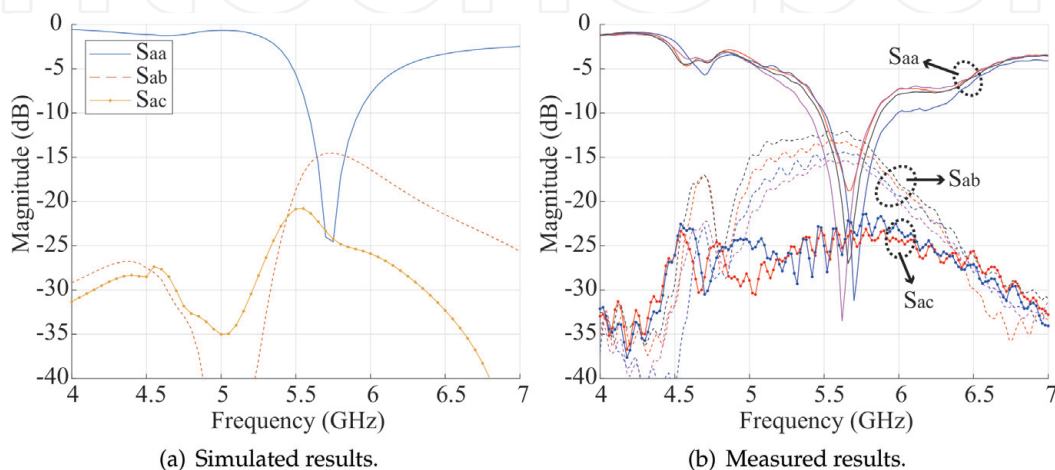


**Figure 7.**  
S-parameters of four-port integrated antenna. (a) Simulated results and (b) measured results.

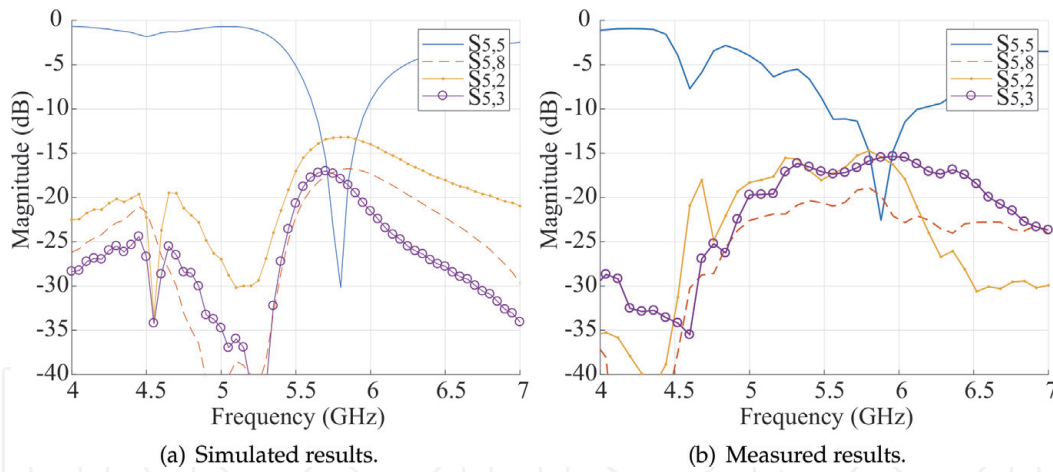


**Figure 8.** *S*-parameters of integrated antenna-based  $1 \times 4$  array. (a) Simulated results and (b) measured results.

a symmetric configuration. It is found that the mutual coupling between antenna elements of different array elements is lower by about  $-13$  dB in simulation and measurement results. Thus, it can be noted that the integrated antenna is scalable in the array structure.

The radiation patterns of the integrated antenna are illustrated in **Figure 9**. It is found that the simulated and measured radiation patterns are agreed well. It is shown that the antenna elements radiate to  $y$ -axis in order to support the front area of the antenna structure and have different radiation patterns. The radiation patterns generated by using the transmitting coefficient matrix  $\mathbf{T}$  are similar to the simulated radiation patterns as well. Thus, it can be noted that the radiation patterns of the practical antenna can be described in a mathematical expression.

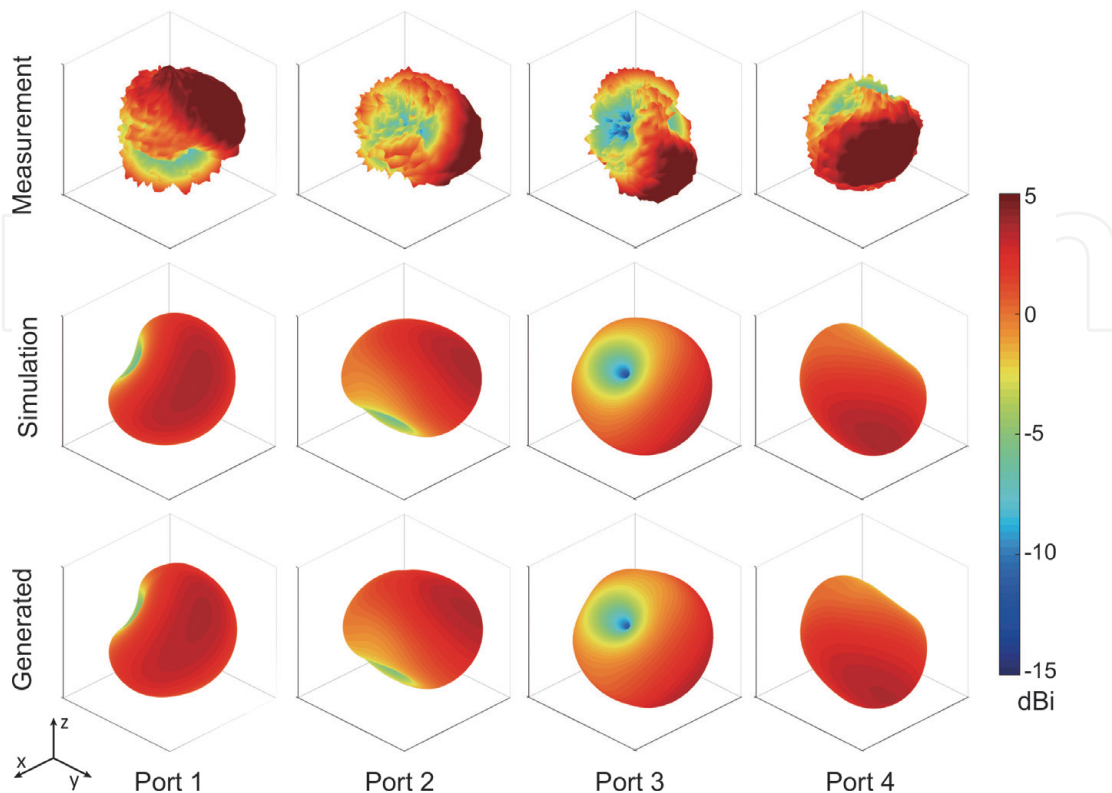


**Figure 9.** Radiation patterns of proposed four-port pattern antenna.

#### 4. Array optimization based on integrated antenna array

It is important to combine the integrated antenna array and the array optimization algorithm. We assume that the integrated antenna array is utilized as a transmit system, and then the channel capacity of the MIMO system may be described as

$$C = \mathbb{E} \left\{ \log \det \left( \mathbf{I}_{N_r} + \frac{\text{SNR}}{N_t} \mathbf{H} \mathbf{W} \mathbf{W}^\dagger \mathbf{H}^\dagger \right) \right\}, \quad (17)$$

where SNR is signal-to-noise ratio and  $\mathbf{W}$  is a precoding matrix [19]. To simplify the optimization problem, we consider that the receive system has ideal channel condition, which means  $\mathbf{R}_{H_r} = \mathbf{I}$ . From (4) and (13), the MIMO channel  $\mathbf{H}$  is given by  $\mathbf{H} = \mathbf{H}_w \mathbf{R}_{H_t}^{1/2}$ , where  $\mathbf{R}_{H_t} = \check{\mathbf{T}}^\dagger \check{\mathbf{R}}_{M_t} \check{\mathbf{T}}$ . There are three variables  $\check{\mathbf{R}}_{M_t}$ ,  $\check{\mathbf{T}}$  and  $\mathbf{W}$  in (17). We can control  $\check{\mathbf{T}}$  and  $\mathbf{W}$  according to  $\check{\mathbf{R}}_{M_t}$  which is given by the channel environment.

However,  $\check{\mathbf{T}}$  and  $\mathbf{W}$  have different characteristics. First,  $\check{\mathbf{T}}$  is determined by the structure of the integrated antenna array, while  $\mathbf{W}$  can be changed in real time. Second,  $\check{\mathbf{T}}$  is dependent on the specification of the integrated antenna such as antenna space, required bandwidth and the number of antenna elements.  $\mathbf{W}$  is dependent on the specification of RF chains such as resolutions of phase shifter and attenuator. Lastly, it is not clear to implement a specific integrated antenna according to an arbitrary  $\check{\mathbf{T}}$ .

Therefore, it is necessary to optimize the  $\check{\mathbf{T}}$  and  $\mathbf{W}$  with different constraints. We study the optimization of  $\mathbf{W}$  under practical  $\check{\mathbf{T}}$ .

##### 4.1 Performance of integrated antenna

In order to show the possibility of the integrated antenna in wireless communication area, we verify the performance of the integrated antenna by optimizing  $\mathbf{W}$  under fixed  $\mathbf{T}$  given by the practical 16-port and 4-port integrated antennas in the previous section.

There are various objective functions for optimization of  $\mathbf{W}$ , such as maximizations of spectral and energy efficiency and minimizations of interference and side lobe level [12]. Here, we consider an objective function as a maximization of spectral efficiency expressed by

$$f = \max_{\text{Tr}\{\mathbf{W}\mathbf{W}^\dagger\}=N_t} C. \quad (18)$$

To obtain the optimum value of  $\mathbf{W}$ , we apply a singular value decomposition (SVD) precoding method into the integrated antenna array [19]. This SVD precoding method provides the precoding matrix  $\mathbf{W} = [\mathbf{v}_1 \cdots \mathbf{v}_{N_t}]$ , where  $\mathbf{U} \mathbf{S} \mathbf{V}^\dagger = \text{svd}(\mathbf{H})$  and  $\mathbf{V} = [\mathbf{v}_1 \cdots \mathbf{v}_{N_t}]$ .

We consider the 16-port integrated antenna as the integrated antenna without array structure. We assume that the receive system has 16 antennas and that the channel is a full-scattering environment, which has the PAS given by

$$p_{\theta_t}(\theta, \phi) = p_{\phi_t}(\theta, \phi) = \frac{1}{2\pi^2}, \theta \in [0, \pi], \phi \in [-\pi, \pi]. \quad (19)$$

The channel capacity of the 16-port integrated antenna is described in **Figure 10**. It is found that the channel capacity of 16-port integrated antenna achieves channel capacity close to that of the ideal 16-port antenna.

#### 4.2 Performance of integrated antenna array

We consider the four-port integrated antenna, which was proposed in Section 3 as the array element of the integrated antenna array. We assume that all antenna arrays have  $N_t = 16$  antenna elements and that the receive system has ideal channel condition which means  $\mathbf{R}_{H_r} = \mathbf{I}_{N_r}$ . We verify the performance of the integrated antenna array compared to two reference arrays as shown in **Figure 11**. The reference arrays are mono-polarization (MPOL) and dual-polarization (DPOL) antenna arrays. The MPOL and DPOL antenna arrays have array elements which are composed of mono-polarization dipole and dual-polarization dipoles, respectively. Then, MPOL, DPOL and integrated antenna arrays have  $B_t = 1, 2$  and  $4$  and  $L_t = 16, 8$  and  $4$ , respectively. Here, we consider a channel model describing an urban macro-cell environment [20].

The channel capacities of the integrated MPOL and DPOL antenna arrays are illustrated in **Figure 12**. Although the integrated antenna array occupies smaller size than the others, the integrated antenna array has higher channel capacity than the MPOL and DPOL antenna arrays. It means that the multiple radiation patterns of various antenna elements for the integrated antenna may enhance the channel capacity without increasing antenna space to utilize spatial gain.

#### 4.3 Further works

To optimize an integrated antenna array in wireless communication area, we study the mathematical optimization of the integrated antenna array. Under assumption of  $\mathbf{W} = \mathbf{I}$ , we can derive an optimization problem given by

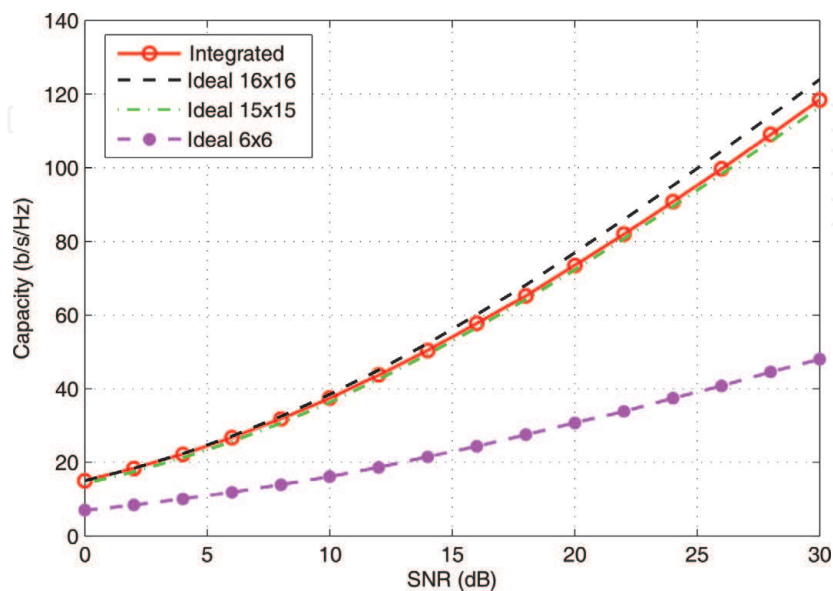


**Figure 10.**  
 Channel capacity of practical 16-port integrated antenna.

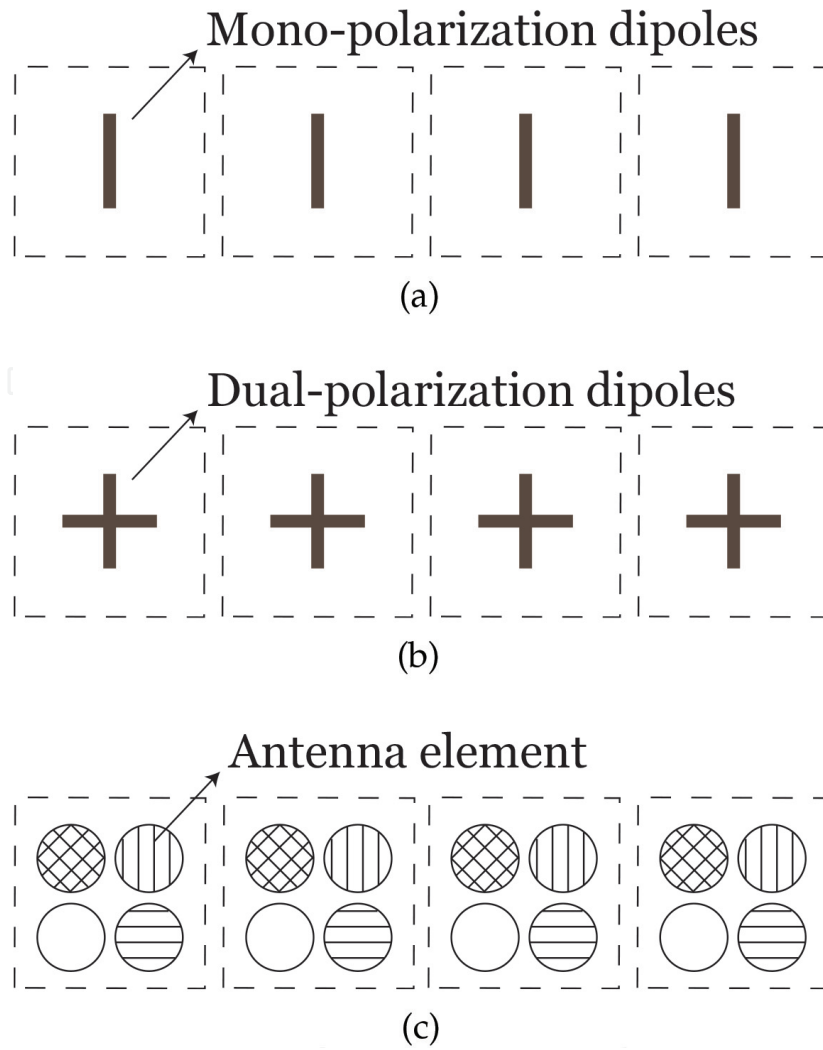


**Figure 11.**  
Configuration of antenna arrays.

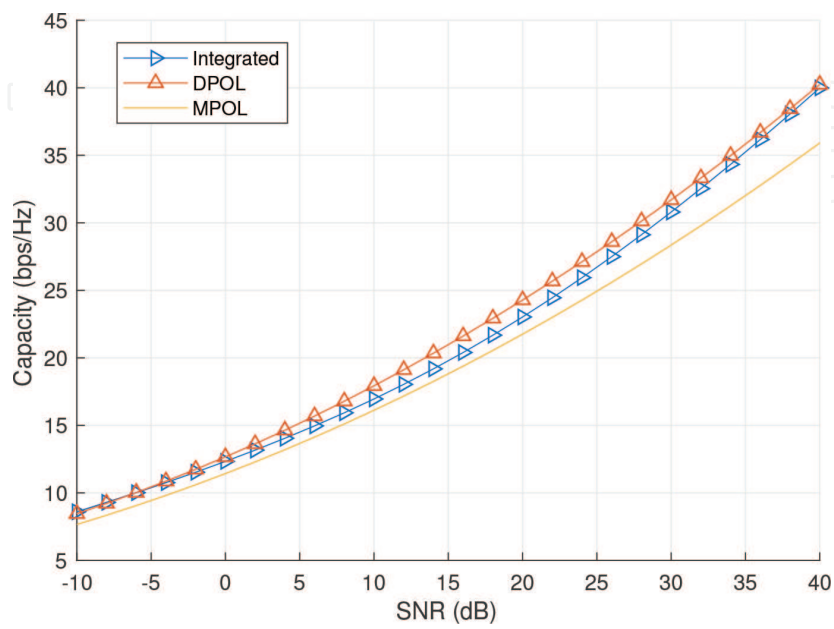


**Figure 12.**  
Channel capacities of various antenna arrays.

$$f = \max_{\text{Tr}\{\mathbf{T}^\dagger\mathbf{T}\}=M_t} \mathbb{E} \left\{ \log \det \left( \mathbf{I}_{N_r} + \frac{\text{SNR}}{N_t} \mathbf{H}\mathbf{H}^\dagger \right) \right\}. \quad (20)$$

However, the achievable  $\mathbf{T}$  is related to various physical parameters such as antenna space and Q-factor. Thus, it is necessary to design the structure of the integrated antenna which has a specific  $\mathbf{T}$ .

On the other hand, there are different constraints and objective functions for  $\mathbf{T}$  and  $\mathbf{W}$  as we mentioned. It is possible to apply various beamforming and precoding methods appropriately according to the structure of the integrated antenna array, such as hybrid-beamforming and low-complex precoding. It is also required to support multiple users with the integrated antenna array.

## 5. Conclusion

We introduced the integrated antenna array for the 5G communication technology and provided the MIMO channel model for the integrated antenna array. We showed that the integrated antenna can be implemented as practical antenna systems for the wireless communication. We also proposed the practical integrated antenna array with the four-port integrated antenna. Based on the MIMO channel model, we explained the optimization problems for the integrated antenna array. The performance of the integrated antenna array was verified compared to dual-polarization antenna array. It has been shown that the integrated antenna array can achieve higher spectral efficiency than the conventional antenna arrays. Therefore, it could be seen that the integrated antenna array would be an attractive solution for the next wireless communication technology.

## A. Appendix

In a source-free region  $V$  filled with a homogeneous medium, the electric field and magnetic field, with assumption of time dependence of  $\exp(-j\omega t)$ , satisfy

$$\nabla \times \nabla \times \mathbf{A}(\mathbf{r}) - k^2 \mathbf{A}(\mathbf{r}) = \mathbf{0}. \quad (21)$$

$\mathbf{A}(\mathbf{r})$  is derivable from the scalar potential  $\Psi(\mathbf{r})$  which satisfies

$$(\nabla^2 + k^2) \Psi(\mathbf{r}) = 0. \quad (22)$$

Consider vector wave functions  $\mathbf{M}(\mathbf{r})$ ,  $\mathbf{N}(\mathbf{r})$  and  $\mathbf{L}(\mathbf{r})$  given by

$$\mathbf{M}(\mathbf{r}) = \nabla \times \mathbf{c}\Psi(\mathbf{r}), \quad \mathbf{N}(\mathbf{r}) = \frac{1}{k} \nabla \times \mathbf{M}(\mathbf{r}), \quad \mathbf{L}(\mathbf{r}) = \Psi(\mathbf{r}), \quad (23)$$

where  $\mathbf{c}$  is a pilot vector. Here,  $\mathbf{M}(\mathbf{r})$  and  $\mathbf{N}(\mathbf{r})$  are divergence-free and orthogonal.  $\mathbf{L}(\mathbf{r})$  is curl-free and orthogonal with  $\mathbf{M}(\mathbf{r})$  and  $\mathbf{N}(\mathbf{r})$ . Then, an arbitrary electromagnetic field can be described with  $\mathbf{M}(\mathbf{r})$  and  $\mathbf{N}(\mathbf{r})$  and  $\mathbf{L}(\mathbf{r})$  [21].

In spherical coordinates, we can obtain the solution to (22) for unbounded media as

$$\Psi(k, \mathbf{r}) = z_n^{(c)}(kr) Y_{nm}(\theta, \phi), \quad (24)$$

where  $z_n^{(c)}$  is the radial function and  $Y_{nm}(\theta, \phi)$  is the complex spherical harmonic function. The radial function  $z_n^{(c)}$  is determined by an upper index ( $c$ ) as one of the following functions:

$$z_n^{(1)}(kr) = j_n(kr) \quad (\text{spherical Bessel function}) \quad (25)$$

$$z_n^{(2)}(kr) = n_n(kr) \quad (\text{spherical Neumann function}) \quad (26)$$

$$z_n^{(3)}(kr) = h_n^{(1)}(kr) = j_n(kr) + jn_n(kr) \quad (\text{spherical Hankel function of the first kind}) \quad (27)$$

$$z_n^{(4)}(kr) = h_n^{(2)}(kr) = j_n(kr) - jn_n(kr) \quad (\text{spherical Hankel function of the second kind}), \quad (28)$$

where  $c = 1$  and  $c = 2$  indicate standing waves and  $c = 3$  and  $c = 4$  indicate an outgoing wave and incoming wave, respectively. The complex spherical harmonic function  $Y_{nm}(\theta, \phi)$  is expressed as

$$Y_{nm}(\theta, \phi) = C_{nm} P_n^m(\cos \theta) e^{jm\phi} = \sqrt{\frac{(n-m)!(2n+1)}{(n+m)!4\pi}} P_n^m(\cos \theta) e^{jm\phi}, \quad (29)$$

where  $P_n^m(\cos \theta)$  is the associated Legendre polynomial,  $C_{nm}$  is a normalization factor,  $n = 0, 1, \dots$  and  $m = -n, -n+1, \dots, 0, 1, \dots, n-1, n$  [10]. The complex spherical harmonic function  $Y_{nm}(\theta, \phi)$  can be defined by the real combinations of the azimuth functions as follows [22]:

$$Y_{\sigma nm}(\theta, \phi) = \sqrt{2} C_{nm} P_n^m(\cos \theta) \begin{cases} \cos m\phi \\ \sin m\phi \end{cases}, \quad (30)$$

where  $m = 0, 1, \dots, n-1, n$  and  $\sigma = e, o$  (even or odd in  $\phi$ ).

The normalized vector spherical harmonics  $\mathbf{A}_{\tau\sigma nm}(\hat{\mathbf{r}})$  can be defined with using the real spherical harmonic function  $Y_{\sigma nm}(\hat{\mathbf{r}}) = \hat{\mathbf{r}} Y_{\sigma nm}(\theta, \phi)$  as follows [11]:

$$\begin{cases} \mathbf{A}_{1\sigma nm}(\hat{\mathbf{r}}) = \frac{1}{\sqrt{n(n+1)}} \nabla \times \mathbf{r} Y_{\sigma nm}(\hat{\mathbf{r}}), \\ \mathbf{A}_{2\sigma nm}(\hat{\mathbf{r}}) = \frac{1}{\sqrt{n(n+1)}} \frac{1}{k} r \nabla Y_{\sigma nm}(\hat{\mathbf{r}}), \\ \mathbf{A}_{3\sigma nm}(\hat{\mathbf{r}}) = \hat{\mathbf{r}} \nabla Y_{\sigma nm}(\hat{\mathbf{r}}). \end{cases} \quad (31)$$

where  $n = 0, 1, \dots$ , and  $m = 0, 1, \dots, n-1, n$  and  $\sigma = e, o$ . In this case, (23) may be modified by

$$\begin{aligned} \mathbf{M}_{\sigma nm}(k, \mathbf{r}) &= \nabla \times \mathbf{r} z_n^{(c)}(kr) Y_{\sigma nm}(\theta, \phi), \\ \mathbf{N}_{\sigma nm}(k, \mathbf{r}) &= \frac{1}{k} \nabla \times \nabla \times \mathbf{r} z_n^{(c)}(kr) Y_{\sigma nm}(\theta, \phi), \\ \mathbf{L}_{\sigma nm}(k, \mathbf{r}) &= \frac{1}{k} \nabla z_n^{(c)}(kr) Y_{\sigma nm}(\theta, \phi). \end{aligned} \quad (32)$$

Because of the orthogonal relationship, furthermore, an arbitrary field  $\mathbf{E}(\mathbf{r})$  can be represented as

$$\mathbf{E}(\mathbf{r}) = \sum_{\sigma=e,o} \sum_{n=1}^{\infty} \sum_{m=0}^m \int_0^{\infty} dk k^2 [a_{\sigma nm}(k) \mathbf{M}_{\sigma nm}(k, \mathbf{r}) + b_{\sigma nm}(k) \mathbf{N}_{\sigma nm}(k, \mathbf{r}) + c_{\sigma nm}(k) \mathbf{L}_{\sigma nm}(k, \mathbf{r})]. \quad (33)$$

From (25) and (32), the outgoing vector waves  $\boldsymbol{\psi}_{\tau\sigma nm}$  are expressed as

$$\begin{cases} \boldsymbol{\psi}_{1\sigma nm}(\theta, \phi) = \nabla \times \mathbf{r} h_n^{(1)}(kr) Y_{\sigma nm}(\theta, \phi), \\ \boldsymbol{\psi}_{2\sigma nm}(\theta, \phi) = \frac{1}{k} \nabla \times \nabla \times \mathbf{r} h_n^{(1)}(kr) Y_{\sigma nm}(\theta, \phi), \end{cases} \quad (34)$$

These spherical vector waves may become the solutions to the vector wave functions  $\mathbf{M}_{\sigma nm}$  and  $\mathbf{N}_{\sigma nm}$ . The outgoing spherical vector waves can be described approximately as

$$\boldsymbol{\psi}_{\tau\sigma nm}(\theta, \phi) = (-j)^{n+2-\tau} \frac{\exp jkr}{kr} \mathbf{A}_{\tau\sigma nm}(\hat{\mathbf{r}}) + o((kr)^{-1}), \quad \tau = 1, 2. \quad (35)$$

The far field is the outgoing spherical vector waves when the  $r$  is a very large value relatively to the wavelength. Therefore, the general expression of the far field can be decomposed approximately as

$$\mathbf{F}(\hat{\mathbf{r}}) = \sum_{\alpha} (-j)^{n+2-\tau} f_{\alpha} \mathbf{A}_{\alpha}(\hat{\mathbf{r}}), \quad (36)$$

where multi-index  $\alpha = 2(n(n+1) - 1 + (-1)^s m) + \tau$  and  $s = 1, 2$  for  $\sigma = e, o$ , respectively.

## Author details

Daehee Park\* and Dong-Ho Cho  
 Korea Advanced Institute of Science and Technology (KAIST), Republic of Korea

\*Address all correspondence to: [indeener@gmail.com](mailto:indeener@gmail.com)

## IntechOpen

© 2018 The Author(s). Licensee IntechOpen. This chapter is distributed under the terms of the Creative Commons Attribution License (<http://creativecommons.org/licenses/by/3.0>), which permits unrestricted use, distribution, and reproduction in any medium, provided the original work is properly cited. 

## References

- [1] Paulraj A, Nabar R, Gore D. Introduction to Space-time Wireless Communications. United Kingdom: Cambridge University Press; 2003
- [2] Larsson EG, Edfors O, Tufvesson F, Marzetta TL. Massive MIMO for next generation wireless systems. *IEEE Communications Magazine*. 2014;**52**(2): 186-195
- [3] Ji H, Kim Y, Lee J, Onggosanusi E, Nam Y, Zhang J, et al. Overview of full-dimension MIMO in LTE-advanced pro. *IEEE Communications Magazine*. 2017; **55**(2):176-184
- [4] Andrews MR, Mitra PP, et al. Tripling the capacity of wireless communications using electromagnetic polarization. *Nature*; 2001;**409**(6818): 316-318
- [5] Poon AS, David N. Degree-of-freedom gain from using polarimetric antenna elements. *IEEE Transactions on Information Theory*. 2011;**57**(9): 5695-5709
- [6] Glazunov AA, Zhang J. Some examples of uncorrelated antenna radiation patterns for MIMO applications. In: *PIERS Proceedings*. 2011. pp. 598-602
- [7] Jeon W, Chung SY. The capacity of wireless channels: A physical approach. In: *Information Theory Proceedings (ISIT), 2013 IEEE International Symposium on IEEE*; 2013. pp. 3045-3049
- [8] Mohammed J. Optimal null steering method in uniformly excited equally spaced linear arrays by optimising two edge elements. *Electronics Letters*. 2017; **53**(13):835-837
- [9] Mohammed JR. Element selection for optimized multi-wide nulls in almost uniformly excited arrays. *IEEE Antennas and Wireless Communication Letters Digital Object Identifier*. 2018; **10**:629-632
- [10] Hansen JE. Spherical Near-field Antenna Measurements. Vol. 26. United Kingdom: Stevenage Herts England Peter Peregrinus Ltd IEE Electromagnetic Waves Series; 1988
- [11] Boström A, Kristensson G, Ström S. Transformation properties of plane, spherical and cylindrical scalar and vector wave functions. *Acoustic, Electromagnetic and Elastic Wave Scattering, Field Representations and Introduction to Scattering*. 1991;**1**: 165-210
- [12] Gustafsson M, Nordebo S. Characterization of MIMO antennas using spherical vector waves. *IEEE Transactions on Antennas and Propagation*. 2006;**54**(9):2679-2682
- [13] Glazunov AA, Gustafsson M, Molisch AF, Tufvesson F, Kristensson G. Spherical vector wave expansion of Gaussian electromagnetic fields for antenna-channel interaction analysis. *IEEE Transactions on Antennas and Propagation*. 2009;**57**(7):2055-2067
- [14] Glazunov A. Expansion of the kronecker and keyhole channels into spherical vector wave modes. *Antennas and Wireless Propagation Letters*. 2011; **10**:1112-1115
- [15] Alayon Glazunov A. A survey of the application of the spherical vector wave mode expansion approach to antenna-channel interaction modeling. *Radio Science*. 2014;**49**(8):663-679
- [16] Chiu CY, Yan JB, Murch RD, Yun JX, Vaughan RG. Design and implementation of a compact 6-port

antenna. *IEEE Antennas and Wireless Propagation Letters*. 2009;**8**:767-770

[17] Park D, Cho DH. Analysis of pattern gain of compact directional 16-port antenna. *IEEE Antennas and Wireless Propagation Letters*. 2015;**14**:902-905

[18] Capobianco AD, Pigozzo FM, Assalini A, Midrio M, Boscolo S, Sacchetto F. A compact MIMO array of planar end-fire antennas for WLAN applications. *IEEE Transactions on Antennas and Propagation*. 2011;**59**(9): 3462-3465

[19] Tse D, Viswanath P. *Fundamentals of Wireless Communication*. United Kingdom: Cambridge University Press; 2005

[20] Glazunov AA, Gustafsson M, Molisch AF, Tufvesson F. Physical modelling of multiple-input multiple-output antennas and channels by means of the spherical vector wave expansion. *IET Microwaves, Antennas and Propagation*. 2010;**4**(6):778-791

[21] Chew WC. *Waves and Fields in Inhomogeneous Media*. United States: IEEE Press; 1995

[22] Whittaker ET, Watson GN. *A Course of Modern Analysis*. United States: Cambridge University Press; 1996